RSC Advances

PAPER

View Article Online
View Journal | View Issue

Cite this: *RSC Adv.*, 2017, **7**, 28797

A $Bi_{7.38}Cr_{0.62}O_{12+x}$ crystal as a novel visible-light-active photocatalyst up to ~650 nm†

W. X. Liao, [ab] X. L. Zhao[ab] and T. S. Wang*[a]

Received 14th March 2017
Accepted 2nd May 2017

DOI: 10.1039/c7ra03058d

rsc.li/rsc-advances

The relatively wide band gap (>2.0 eV) and limited light absorption ranges (only up to 600 nm) of photocatalysts severely restrict the exploitation of solar energy. Herein, we developed a $Bi_{7.38}Cr_{0.62}O_{12+x}$ crystal photocatalyst with a narrow band gap of 1.98 eV and a broad light absorption range of ~650 nm. Unlike other broad light absorption range photocatalysts (up to ~650 nm) such as red phosphorus, Fe_2O_3, and CdSe, which are either unstable or show low photocatalytic performances, the as-synthesized $Bi_{7.38}Cr_{0.62}O_{12+x}$ crystal photocatalyst exhibits a steady photocatalytic activity for the decomposition of methylene blue, methyl blue, and phenol, and production of O_2.

1. Introduction

With the increasing awareness of the environmental degradation and energy crisis, significant effort has been devoted to taking advantage of visible light-active photocatalysts with an excellent photocatalytic activity for environmental remediation and solar energy utilization.[1–4] However, most of the visible light-active photocatalysts explored to date have relatively wide band gaps and limited light absorption ranges. Some of these photocatalysts are C_3N_4 (absorption up to ~450 nm),[5,6] Ga_x-$Zn_{1-x}(N_xO_{1-x})$ (~470 nm),[7,8] elemental sulfur (~480 nm),[9] CdS (~520 nm),[10,11] and $Zn_xCd_{1-x}S$ (~500 nm).[12,13] On the other hand, photocatalysts, such as red phosphorus,[14] Fe_2O_3,[15,16] and CdSe,[17] with narrower band gaps have broad absorption ranges reaching up to ~650 nm; however, these photocatalysts are either unstable under illumination or have low photocatalytic performances. Thus, several approaches have been explored to extend the absorption range of the photocatalysts: incorporating oxygen vacancies,[18,19] doping with metal elements,[20,21] combining with narrow band gap semiconductors,[22,23] and sensitization with narrow band gap quantum dots or dye molecules.[24,25] However, these type of photocatalysts are mostly active during interband transitions. Furthermore, defects or interfaces tend to be the recombination centres for the photogenerated carriers. Thus, it remains a great challenge to develop highly efficient and stable photocatalysts with broad light absorption ranges reaching up to ~650 nm.

Bi-based semiconductors such as BiOX (X = Cl, Br, and I),[26] $BiVO_4$,[27] Bi_2WO_6,[28] Bi_2MoO_6,[29] Bi_2O_3,[30] Bi_2S_3,[31] and bismuth titanate[32] are particularly attractive as new promising candidates for visible-light-active photocatalysts because of their high photocatalytic performance. In this study, we report a new type of Bi-based visible light-active photocatalyst, $Bi_{7.38}Cr_{0.62}O_{12+x}$, which has a narrow band gap of 1.98 eV and exhibits photoelectric response until 647.4 nm. Moreover, $Bi_{7.38}Cr_{0.62}O_{12+x}$ has a steady photocatalytic activity for the decomposition of methylene blue, methyl blue, and phenol, and production of O_2.

2. Experimental

2.1 Chemicals and materials

$Bi(NO_3)_3 \cdot 5H_2O$ (AR, 99.0%), $Cr(NO_3)_3 \cdot 9H_2O$ (AR, 99.0%), $AgNO_3$ (AR, 99.0%), methylene blue (AR), and methyl blue (AR) were purchased from Aladdin Reagent Company. Acetic acid (AR, 99.8%) and methanol (AR, 99.5%) were purchased from Beijing Chemical Reagent Company. All the chemicals were used as purchased without any further purification. Commercial P25 TiO_2 was purchased from Degussa AG, Germany.

2.2 Synthesis of the $Bi_{7.38}Cr_{0.62}O_{12+x}$ crystal

In the typical synthesis of the $Bi_{7.38}Cr_{0.62}O_{12+x}$ crystal, 6 mmol of $Bi(NO_3)_3 \cdot 5H_2O$ and 0.5 mmol of $Cr(NO_3)_3 \cdot 9H_2O$ were dissolved in 50 mL of acetic acid and vigorously stirred at 250 °C to volatilize acetic acid. The mixture was heated to 600 °C at a rate of 5 °C min^{-1} in a muffle furnace and maintained at this temperature for 5 h. Then, the $Bi_{7.38}Cr_{0.62}O_{12+x}$ crystal was obtained after cooling down the mixture to room temperature.

2.3 Synthesis of N-doped P25

N-doped P25 was prepared by treating the P25 samples in a tubular furnace under an NH_3 flow (purity 99.99%) at a high temperature of 500 °C for 4 h. The NH_3 flow was applied for

[a]State Key Laboratory of Applied Optics, Changchun Institute of Optics, Fine Mechanics and Physics, Chinese Academy of Sciences, Changchun, Jilin 130033, China. E-mail: wangtaisheng@sina.com

[b]University of Chinese Academy of Sciences, Beijing 100039, China

† Electronic supplementary information (ESI) available: More Tauc plots, SEM, BET and photocatalytic degradation of $Bi_{7.38}Cr_{0.62}O_{12+x}$ crystal. See DOI: 10.1039/c7ra03058d

30 min before the heat treatment to remove the air and maintained until the products were cooled down to room temperature.

2.4 Characterizations

Scanning electron microscopy (SEM) images were obtained using JEOL JSM 4800F. Transmission electron microscopy (TEM) images were obtained using an FEI Tecnai G2, operated at 200 kV. Ultraviolet photoelectron spectroscopy (UPS) measurements were performed using an unfiltered He I (21.22 eV) gas discharge lamp and a total instrumental energy resolution of 100 meV. The crystalline structure was investigated *via* an X-ray diffractometer (XRD) (Bruker AXS D8 Focus) using Cu K_α radiation (λ = 1.54056 Å). The Brunauer–Emmett–Teller (BET) specific surface area was measured using a Micromeritics Gemini V surface area and pore size analyzer. UV-vis absorption spectra were obtained using a UV-3600 UV-vis-NIR scanning spectrophotometer (Shimadzu). X-ray photoelectron spectroscopy (XPS) measurements were performed using an ESCALABMKII spectrometer with an Al-K_α (1486.6 eV) achromatic X-ray source.

2.5 Photocatalytic decomposition of methylene blue

The visible light photocatalytic activity of the $Bi_{7.38}Cr_{0.62}O_{12+x}$ crystal was evaluated by monitoring the decomposition of methylene blue and methyl blue in an aqueous solution under visible light irradiation from a 300 W Xe lamp (PLS-SXE 300, Beijing Trusttech Co. Ltd, China) with a UVCUT-420 nm filter (Newport). A pyrex glass vessel was used as the photoreactor. The $Bi_{7.38}Cr_{0.62}O_{12+x}$ crystal (200 mg) was mixed with a methylene blue solution (50 mL, 10 ppm). After stirring for 60 min in dark to reach the adsorption equilibrium, the solution was illuminated under visible light irradiations. The concentration of the aqueous solution of methylene blue was determined using a UV-vis spectrophotometer *via* measuring the peak intensity at 664 nm.

2.6 Photocatalytic decomposition of methyl blue

The $Bi_{7.38}Cr_{0.62}O_{12+x}$ crystal (200 mg) was mixed with a methyl blue solution (50 mL, 30 ppm). After stirring for 60 min in dark to reach the adsorption equilibrium, the solution was illuminated under visible light irradiations. The concentration of the aqueous solution of methyl blue was determined using a UV-vis spectrophotometer *via* measuring the peak intensity at 601 nm. To further determine the probable active species for photocatalytic decomposition, 100 mg of $AgNO_3$ (electron scavenger) and 5 mL of methanol (hole scavenger) were added.

2.7 Photocatalytic decomposition of phenol

The $Bi_{7.38}Cr_{0.62}O_{12+x}$ crystal (200 mg) crystal was mixed with a phenol solution (50 mL, 200 μmol L^{-1}). After stirring for 60 min in dark to reach the adsorption equilibrium, the solution was illuminated under visible light irradiations. The concentration of the aqueous solution of phenol was determined using a UV-vis spectrophotometer *via* measuring the peak intensity at 270 nm.

2.8 Photocatalytic O_2 production measurements

The $Bi_{7.38}Cr_{0.62}O_{12+x}$ crystal (50 mg) was added to a $AgNO_3$ solution (100 mL, 0.1 M) within a closed gas circulation system (Perfect Light Company Labsolar-III (AG)). This mixture was exposed to UV-vis and visible light irradiation from a 300 W Xe lamp (PLS-SXE 300, Beijing Trusttech Co. Ltd, China) without and with an UVCUT-420 nm filter (Newport). The evolved gases were detected *in situ* using an online gas chromatograph (GC-2014C, Shimadzu) equipped with a thermal conductivity detector (TCD).

2.9 Surface photovoltage measurements

The surface photovoltage (SPV) measurement system consisted of a source of monochromatic light, a lock-in amplifier (SR 830-DSP) with a light chopper (SR 540), and a sample chamber. The monochromatic light is provided by a 300 W Xe lamp (PLS-SXE 300, Beijing Trusttech Co. Ltd, China) and a monochromator (SBP500, Zolix). All measurements were performed at room temperature and under ambient pressure, and samples were not pretreated prior to the SPV measurements.

2.10 Detection of the hydroxyl radicals

The ESR signal of the radicals spin-trapped by 5,5-dimethyl-1-pyrroline-N-oxide (DMPO) was measured *via* a Bruker ESP 300A spectrometer. The irradiation source was a 300 W xenon lamp with a cut-off filter (λ > 420 nm). The settings for the ESR spectrometer were as follows: center field, 3510.00 G; microwave frequency, 9.79 GHz; and power, 5.05 mW.

3. Results and discussion

The synthesis of the $Bi_{7.38}Cr_{0.62}O_{12+x}$ crystal consisted a solid phase reaction in which $Bi(NO_3)_3$ and $Cr(NO_3)_3$ acted as the precursors. As shown in Fig. 1A, in the XRD patterns of the as-synthesized $Bi_{7.38}Cr_{0.62}O_{12+x}$ crystal, the diffraction peaks at 27.72, 32.61, 45.71, 53.35, and 55.26 degrees, ascribed to the (2 0 1), (2 2 0), (2 2 2), (2 0 3), and (4 2 1) planes of $Bi_{7.38}Cr_{0.62}O_{12+x}$, were indexed to the tetragonal phase (JCPDS no. 50-0373). The EDAX spectrum (Fig. 1B) indicated that the mole ratio of Bi, Cr, and O was close to the stoichiometric ratio of 12 : 1 : 19. Diffused reflective UV-vis spectroscopy spectrum is presented in Fig. 1C. The oranger powders display a strong absorption band in the visible light region. The bandgap E_g of $Bi_{7.38}Cr_{0.62}O_{12+x}$ was calculated to be 1.98 eV from the Tauc plot (Fig. S1†). Surface photovoltage spectroscopy (SPS) is a powerful tool to characterize charge separation at the nanoscale.[33] As shown in Fig. 1D, the SPS spectrum presents an active negative surface photovoltage (SPV) response, indicating that $Bi_{7.38}Cr_{0.62}O_{12+x}$ is a p-type semiconductor. The SPV response reaches 647.4 nm, which is in agreement with the absorption spectrum (Fig. 1C). Furthermore, the strong SPV response indicates that the generated carriers can be efficiently separated, and therefore, $Bi_{7.38}Cr_{0.62}O_{12+x}$ may have a good photocatalytic activity.

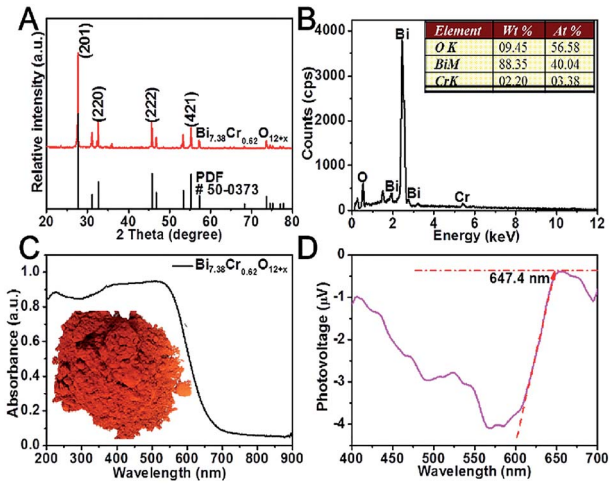

Fig. 1 X-ray diffraction patterns (A), EDAX spectrum (B), diffusion reflection UV-vis spectrum (C), and surface photovoltage spectroscopy spectrum (SPS) (D) of the $Bi_{7.38}Cr_{0.62}O_{12+x}$ crystal. The inset of C is an image of the $Bi_{7.38}Cr_{0.62}O_{12+x}$ crystal.

The FE-SEM images (Fig. S2†) show that the $Bi_{7.38}Cr_{0.62}O_{12+x}$ crystal is composed of blocks of several microns. The lattice fringe space of 0.322 nm, as observed in the HRTEM image (Fig. 2B), is characteristic of the (2 0 1) plane of the tetragonal phase of $Bi_{7.38}Cr_{0.62}O_{12+x}$. The Brunauer–Emmett–Teller (BET) surface area and pore size of the sample were calculated from the N_2 adsorption–desorption isotherms, as shown in Fig. S3.† The type-III isotherm with a type-D hysteresis loop indicated a macroporous structure,[34–36] while the BET surface area was determined to be 1.89 $m^2\ g^{-1}$.

XPS (X-ray photoelectron spectroscopy) is a powerful technique to investigate the chemical states of a material. The Bi 4f and Cr 2p high-resolution XPS spectra of the $Bi_{7.38}Cr_{0.62}O_{12+x}$ crystal are shown in Fig. 3. The Bi 4f spectra was resolved into two Gaussian peaks. The peaks at 158.6 and 163.8 eV can be assigned to the Bi 4f 7/2 and Bi 4f 5/2 regions of the bismuth oxide species.[37,38] The Cr 2p high resolution XPS spectra could be fitted into two Gaussian peaks at 576.3 eV and 579.8 eV. The Cr 2p 3/2 peak at 576.3 eV is usually assigned to the Cr(III) species, such as Cr_2O_3,[39–41] while the component at 579.8 eV is associated with the Cr(VI) species, such as K_2CrO_4 or $K_2Cr_2O_7$.[42] Thus, the XPS results confirmed that Cr(VI) was the main valence state in the $Bi_{7.38}Cr_{0.62}O_{12+x}$ crystal.

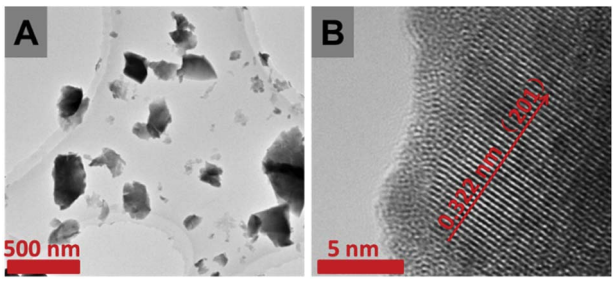

Fig. 2 Low resolution TEM image (A) and HRTEM image (B) of the $Bi_{7.38}Cr_{0.62}O_{12+x}$ crystal.

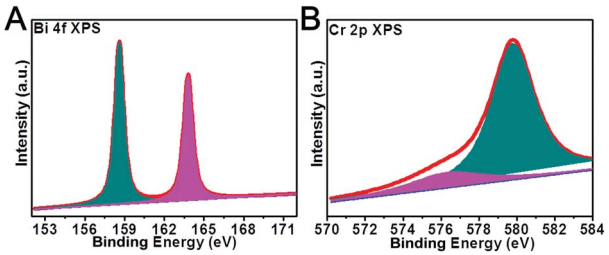

Fig. 3 Bi 4f (A) and Cr 2p (B) high resolution XPS spectra of the $Bi_{7.38}Cr_{0.62}O_{12+x}$ crystal. The Bi 4f XPS spectrum can be deconvoluted into two Gaussian peaks, located at around 158.6 eV and 163.8 eV. The Cr 2p XPS spectrum can be fitted into two Gaussian peaks at 576.3 eV and 579.8 eV.

The visible-light photocatalytic activity of the $Bi_{7.38}Cr_{0.62}O_{12+x}$ crystal was estimated based on the photocatalytic decomposition of methylene blue, methyl blue, and phenol in an aqueous solution under visible light irradiation from a 300 W Xe lamp (PLS-SXE 300, Beijing Trusttech Co. Ltd, China) with a UVCUT-420 nm filter (Newport). As shown in Fig. 4 and S4–S6,† methylene blue, methyl blue, and phenol presented a negligible self-degradation. Photodegradation was completed after 80 minutes for methylene blue and methyl blue, and after 150 minutes for phenol. By contrast, N-doped P25 showed a relatively lower photocatalytic activity, with only about 30–40% of photodegradation. Furthermore, the photocatalytic degradation at $\lambda > 420$ nm was measured for several successive cycles, and the results are shown in Fig. 5. After five cycles, no loss in the photocatalytic activity was observed. Fig. 6 shows the O_2 production from the $Bi_{7.38}Cr_{0.62}O_{12+x}$ crystal under UV-vis light and visible light irradiation. The O_2 production rate was 9.69 μmol h^{-1} under UV-vis and 3.99 μmol h^{-1} at $\lambda > 420$ nm for 50 mg of $Bi_{7.38}Cr_{0.62}O_{12+x}$ in 100 mL of 0.1 M $AgNO_3$ solution as an electron scavenger. These photocatalytic experiments demonstrated that the $Bi_{7.38}Cr_{0.62}O_{12+x}$ crystal is a stable and efficient visible light-active photocatalyst.

To determine the probable active species involved in the photocatalytic decomposition, 100 mg of $AgNO_3$ (electron scavenger) and 5 mL of methanol (hole scavenger) were added. As shown in Fig. S7,† when 100 mg of $AgNO_3$ was added, the photodegradation was clearly accelerated and completed after 60 minutes, with the rate constant showing a one-time improvement. As an electron scavenger, $AgNO_3$ can rapidly

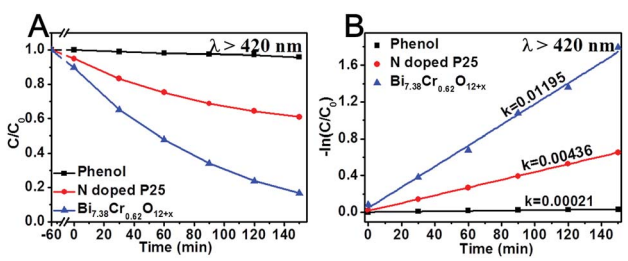

Fig. 4 Photocatalytic degradation at $\lambda > 420$ nm of phenol with N-doped P25 and the $Bi_{7.38}Cr_{0.62}O_{12+x}$ crystal.

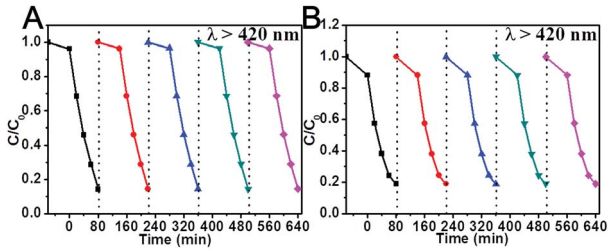

Fig. 5 Photocatalytic degradation at $\lambda > 420$ nm of methylene blue (A) and methyl blue (B) with $Bi_{7.38}Cr_{0.62}O_{12+x}$ after several cycles.

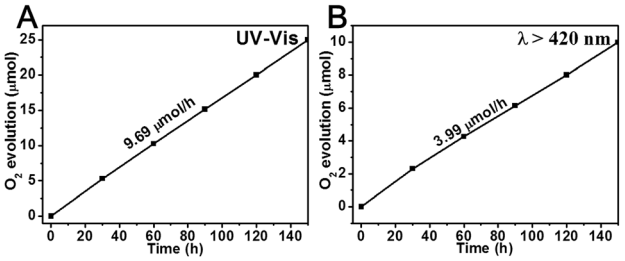

Fig. 6 O_2 production of the $Bi_{7.38}Cr_{0.62}O_{12+x}$ crystal under UV-vis light (A) and visible light (B) irradiation.

capture the generated electrons, leading to a higher separation efficiency of the photogenerated carriers and a longer lifetime of the photogenerated holes.[43,44] The photodegradation is obviously suppressed by the addition of methanol (hole scavenger).[45,46] These results verify that holes and hydroxyl radicals are the main active species oxidizing the adsorbed organic pollutants.[47,48] These species are also reported to be the dominant active species in TiO_2.[1,49] To further verify the generation of hydroxyl radicals in the photodegradation reaction, we measured the ESR signal of the radicals spin-trapped by DMPO, as shown in Fig. 7. Under visible light irradiation, four characteristic peaks with a standard intensity ratio of 1 : 2 : 2 : 1 were clearly observed,[50,51] which could be ascribed to ·DMPO-OH. By contrast, no ESR signal was detected under the dark condition.

To elucidate the origin of the band gap in $Bi_{7.38}Cr_{0.62}O_{12+x}$, we examined the electronic structure of $Bi_{7.38}Cr_{0.62}O_{12+x}$ by density functional theory, as shown in Fig. S8.† The density of states (DOS) calculations indicated that the valence band maximum (VBM) originated from the O 2p state, whereas the conduction

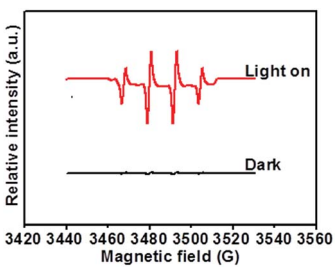

Fig. 7 DMPO spin-trapping ESR spectra of $Bi_{7.38}Cr_{0.62}O_{12+x}$ for ·DMPO-OH.

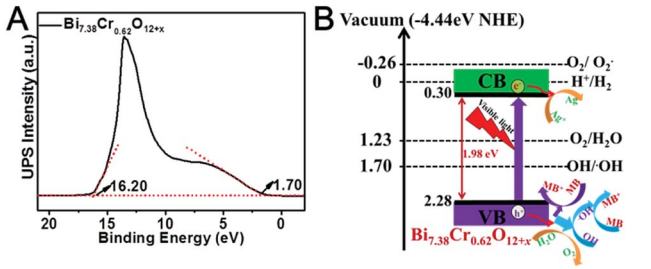

Fig. 8 Ultraviolet photoelectron spectroscopy (UPS) (A) and possible photocatalytic mechanism of the $Bi_{7.38}Cr_{0.62}O_{12+x}$ crystal (B).

band minimum (CBM) was mainly contributed by the Cr 3d and Bi 6p states. The UPS spectra (Fig. 8A) was utilized to confirm the valence band energy (E_v) of the $Bi_{7.38}Cr_{0.62}O_{12+x}$ crystal, which was computed to be 6.72 eV (*versus* vacuum level) by subtracting the width of the He I UPS spectra from the excitation energy (21.22 eV).[52,53] According to the reference standard, for which 0 V *versus* RHE (reversible hydrogen electrode) equals −4.44 eV *versus* the vacuum level,[54,55] E_v was finally estimated to be 2.28 eV *versus* RHE. The conduction band energy E_c was thus calculated to be 0.30 *versus* RHE from $E_v - E_g$. The possible photocatalytic mechanism of the $Bi_{7.38}Cr_{0.62}O_{12+x}$ crystal is shown in Fig. 8B. The valence band energy (E_v) is 0.58 eV higher than that of OH/·OH (1.70 V), and 1.05 eV higher than that of O_2/H_2O (1.23 V). Thus, on the one hand, the generated holes have enough oxidizing power to oxidize adsorbed methylene blue, methyl blue, phenol, and water. On the other hand, the generated holes also have enough oxidizing power to react with OH to produce active hydroxyl radicals that can in turn oxidize the adsorbed methylene blue, methyl blue, and phenol.[47]

4. Conclusions

In summary, we prepared a new type of Bi-based visible light-active photocatalyst, $Bi_{7.38}Cr_{0.62}O_{12+x}$, by a solid phase reaction with $Bi(NO_3)_3$ and $Cr(NO_3)_3$ as the precursors. The XRD and EDAX results confirmed that $Bi_{7.38}Cr_{0.62}O_{12+x}$ was synthesized. The SEM and TEM images show that the crystal is composed of blocks of several microns. The UV-vis DRS spectrum presents a strong visible light absorption band. The XPS results confirmed that Cr(VI) is the main valence state in the $Bi_{7.38}Cr_{0.62}O_{12+x}$ crystal. The photocatalytic decomposition of methylene blue and methyl blue, as well as the photocatalytic production of O_2 indicate that the $Bi_{7.38}Cr_{0.62}O_{12+x}$ crystal is a stable visible light-active photocatalyst. The holes and hydroxyl radicals are the main active species that can oxidize the adsorbed organic pollutants.

Acknowledgements

This work was supported by the National Natural Science Foundation of China (NSFC) under grant no. 61274122, 61361166004, 61475156, 61490712 and 61377068, the Jilin Province and the Technology Development Plan under grant no. 20100351 and 20120323, and the Changchun Science and

Technology Plan under grant no. 2013269, and the Youth Innovation Promotion Association of CAS under grant no. 2014193.

References

1 M. R. Hoffmann, S. T. Martin, W. Choi and D. W. Bahnemann, *Chem. Rev.*, 1995, **95**, 69–96.
2 C. Chen, W. Ma and J. Zhao, *Chem. Soc. Rev.*, 2010, **39**, 4206–4219.
3 H. Wang, L. Zhang, Z. Chen, J. Hu, S. Li, Z. Wang, J. Liu and X. Wang, *Chem. Soc. Rev.*, 2014, **43**, 5234–5244.
4 K. Rajeshwar and N. R. De Tacconi, *Chem. Soc. Rev.*, 2009, **38**, 1984–1998.
5 X. Wang, K. Maeda, A. Thomas, K. Takanabe, G. Xin, J. M. Carlsson, K. Domen and M. Antonietti, *Nat. Mater.*, 2009, **8**, 76–80.
6 X. Chen, J. Zhang, X. Fu and X. Wang, *J. Am. Chem. Soc.*, 2009, **131**(33), 11658–11659.
7 K. Maeda, T. Takata, M. Hara, N. Saito, Y. Inoue, H. Kobayashi and K. Domen, *J. Am. Chem. Soc.*, 2005, **127**, 8286.
8 K. Maeda, K. Teramura, D. Lu, T. Takata, N. Saito, Y. Inoue and K. Domen, *Nature*, 2006, **440**, 295.
9 G. Liu, P. Niu, L. Yin and H.-M. Cheng, *J. Am. Chem. Soc.*, 2012, **134**, 9070–9073.
10 Y. Hu, X. Gao, L. Yu, Y. Wang, J. Ning, S. Xu and X. W. D. Lou, *Angew. Chem.*, 2013, **125**, 5746.
11 D. Jing and L. Guo, *J. Phys. Chem. B*, 2006, **110**, 11139.
12 Q. Li, H. Meng, J. Yu, W. Xiao, Y. Zheng and J. Wang, *Chem.–Eur. J.*, 2014, **20**, 1176.
13 J. Ran, J. Zhang, J. Yu and S. Z. Qiao, *ChemSusChem*, 2014, **7**, 3426.
14 F. Wang, W. K. H. Ng, C. Y. Jimmy, H. Zhu, C. Li, L. Zhang, Z. Liu and Q. Li, *Appl. Catal., B*, 2012, **111**, 409–414.
15 M. Fouda, M. ElKholy, S. Mostafa, A. Hussien, M. Wahba and M. El-Shahat, *Adv. Mater. Lett.*, 2013, **4**(5), 347–353.
16 M. Fouda, M. El-Kholy, S. Moustafa, A. Hussien, M. Wahba and M. El-Shahat, *Int. J. Inorg. Chem.*, 2012, **2012**, 1–9.
17 W. Huckle, G. F. Swigert and S. E. Wiberley, *Ind. Eng. Chem. Prod. Res. Dev.*, 1966, **5**(4), 362–366.
18 H. Tan, Z. Zhao, M. Niu, C. Mao, D. Cao, D. Cheng, P. Feng and Z. Sun, *Nanoscale*, 2014, **6**, 10216–10223.
19 Z. Wang, C. Yang, T. Lin, H. Yin, P. Chen, D. Wan, F. Xu, F. Huang, J. Lin and X. Xie, *Energy Environ. Sci.*, 2013, **6**, 3007–3014.
20 R. Konta, T. Ishii, H. Kato and A. Kudo, *J. Phys. Chem. B*, 2004, **108**, 8992–8995.
21 R. Niishiro, H. Kato and A. Kudo, *Phys. Chem. Chem. Phys.*, 2005, **7**, 2241–2245.
22 D. Wang, T. Kako and J. Ye, *J. Phys. Chem. C*, 2009, **113**, 3785–3792.
23 S. Song, L. Xu, Z. He, J. Chen, X. Xiao and B. Yan, *Environ. Sci. Technol.*, 2007, **41**, 5846–5853.
24 F. Wang, Y. Liu, Z. Ma, H. Li, Z. Kang and M. Shen, *New J. Chem.*, 2013, **37**, 290–294.
25 Y. Diamant, S. Chen, O. Melamed and A. Zaban, *J. Phys. Chem. B*, 2003, **107**, 1977–1981.
26 H. Cheng, B. Huang and Y. Dai, *Nanoscale*, 2014, **6**, 2009–2026.
27 R. Li, F. Zhang, D. Wang, J. Yang, M. Li, J. Zhu, X. Zhou, H. Han and C. Li, *Nat. Commun.*, 2013, **4**, 1432.
28 J. Tian, Y. Sang, G. Yu, H. Jiang, X. Mu and H. Liu, *Adv. Mater.*, 2013, **25**, 5075–5080.
29 G. Tian, Y. Chen, W. Zhou, K. Pan, Y. Dong, C. Tian and H. Fu, *J. Mater. Chem.*, 2011, **21**, 887–892.
30 L. Zhou, W. Wang, H. Xu, S. Sun and M. Shang, *Chem.–Eur. J.*, 2009, **15**, 1776–1782.
31 Z. Liu, S. Peng, Q. Xie, Z. Hu, Y. Yang, S. Zhang and Y. Qian, *Adv. Mater.*, 2003, **15**, 936–940.
32 W. F. Yao, H. Wang, X. H. Xu, X. F. Cheng, J. Huang, S. X. Shang, X. N. Yang and M. Wang, *Appl. Catal., A*, 2003, **243**, 185–190.
33 L. Kronik and Y. Shapira, *Surf. Sci. Rep.*, 1999, **37**, 1–206.
34 D. Liu, Y. Yao, D. Tang, S. Tang, Y. Che and W. Huang, *Int. J. Coal Geol.*, 2009, **79**, 97–112.
35 M. Khalfaoui, S. Knani, M. Hachicha and A. B. Lamine, *J. Colloid Interface Sci.*, 2003, **263**, 350–356.
36 J. Wang, X. Yang, D. Wu, R. Fu, M. S. Dresselhaus and G. Dresselhaus, *J. Power Sources*, 2008, **185**, 589–594.
37 C. Wang, C. Shao, Y. Liu and L. Zhang, *Scr. Mater.*, 2008, **59**, 332–335.
38 Y. Schuhl, H. Baussart, R. Delobel, M. Le Bras, J.-M. Leroy, L. Gengembre and J. Grimblot, *J. Chem. Soc., Faraday Trans. 1*, 1983, **79**, 2055–2069.
39 I. Grohmann, E. Kemnitz, A. Lippitz and W. Unger, *Surf. Interface Anal.*, 1995, **23**, 887–891.
40 R. Kirby, E. Garwin, F. King and A. Nyaiesh, *J. Appl. Phys.*, 1987, **62**, 1400–1405.
41 F. Werfel, *Phys. Scr.*, 1983, **28**, 92.
42 S. Suzuki, M. Oku and Y. Waseda, *Surf. Interface Anal.*, 1997, **25**, 161–166.
43 A. Sclafani, L. Palmisano and E. Davi, *J. Photochem. Photobiol., A*, 1991, **56**, 113–123.
44 A. Kudo, K. Ueda, H. Kato and I. Mikami, *Catal. Lett.*, 1998, **53**, 229–230.
45 A. Yamakata, T.-A. Ishibashi and H. Onishi, *J. Phys. Chem. B*, 2002, **106**, 9122–9125.
46 H. Dotan, K. Sivula, M. Grätzel, A. Rothschild and S. C. Warren, *Energy Environ. Sci.*, 2011, **4**, 958–964.
47 C. Pan and Y. Zhu, *Environ. Sci. Technol.*, 2010, **44**, 5570–5574.
48 Y. Lv, C. Pan, X. Ma, R. Zong, X. Bai and Y. Zhu, *Appl. Catal., B*, 2013, **138**, 26–32.
49 H. Fu, C. Pan, W. Yao and Y. Zhu, *J. Phys. Chem. B*, 2005, **109**, 22432–22439.
50 R. Li, Y. Weng, X. Zhou, X. Wang, Y. Mi, R. Chong and C. Li, *Energy Environ. Sci.*, 2015, **8**(8), 2377–2382.
51 X. Xiao, J. Jiang and L. Zhang, *Appl. Catal., B*, 2013, **142**, 487–493.
52 J. Liu, Y. Liu, N. Liu, Y. Han, X. Zhang, H. Huang, Y. Lifshitz, S.-T. Lee, J. Zhong and Z. Kang, *Science*, 2015, **347**, 970–974.
53 W.-J. Chun, A. Ishikawa, H. Fujisawa, T. Takata, J. N. Kondo, M. Hara, M. Kawai, Y. Matsumoto and K. Domen, *J. Phys. Chem. B*, 2003, **107**, 1798–1803.
54 Y. Matsumoto, *J. Solid State Chem.*, 1996, **126**, 227–234.
55 C. G. Van de Walle and J. Neugebauer, *Nature*, 2003, **423**, 626–628.